Received: 28 April 2020 | Revised: 20 August 2020 | Accepted: 20 August 2020

DOI: 10.1096/fj.202000994RR

RESEARCH ARTICLE

THE FASEB JOURNAL

The role of neutrophil extracellular traps and TLR signaling in skeletal muscle ischemia reperfusion injury

Nicole J. Edwards[1] | Charles Hwang[1] | Simone Marini[1] | Chase A. Pagani[1] | Philip J. Spreadborough[2] | Cassie J. Rowe[2] | Pauline Yu[1] | Annie Mei[1] | Noelle Visser[1] | Shuli Li[1] | Geoffrey E. Hespe[1] | Amanda K. Huber[1] | Amy L. Strong[1] | Miriam A. Shelef[3] | Jason S. Knight[4] | Thomas A. Davis[2] | Benjamin Levi[1,5]

[1]Department of Surgery, University of Michigan, Ann Arbor, MI, USA

[2]Department of Surgery, Uniformed Services University of the Health Sciences, Bethesda, MD, USA

[3]Division of Rheumatology, University of Wisconsin and William S. Middleton Memorial Veterans Hospital, Madison, WI, USA

[4]Department of Internal Medicine, University of Michigan, Ann Arbor, MI, USA

[5]Department of Surgery, University of Texas Southwestern Medical Center, Dallas, TX, USA

Correspondence
Benjamin Levi, Lee-Hudson Professor and Division Chief of General Surgery; Director, Center for Organogenesis and Trauma, University of Texas Southwestern Medical Center, 5323 Harry Hines Blvd, Dallas, TX 75390-9158, USA.
Email: benjamin.levi@UTSouthwestern.edu

Funding information
NJE was supported by a Ruth L. Kirschstein Institutional National Research Service Award Postdoctoral fellowship (T32-HD007505). CH was supported by a Howard Hughes Medical Institute Medical Research Fellowship. MS was supported by National Institutes of Health NIAMS K08 AR065500. BL was supported or partially supported by National Institutes of Health (NIH) R01GM123069, R01AR071379, American College of Surgeons Clowes Award, US Department of Defense Grants W81XWH-18-1-0653 (OR170174) and W81XWH-17-1-0655 (OR160105).

Abstract

Ischemia reperfusion (IR) injury results in devastating skeletal muscle fibrosis. Here, we recapitulate this injury with a mouse model of hindlimb IR injury which leads to skeletal muscle fibrosis. Injury resulted in extensive immune infiltration with robust neutrophil extracellular trap (NET) formation in the skeletal muscle, however, direct targeting of NETs via the peptidylarginine deiminase 4 (PAD4) mechanism was insufficient to reduce muscle fibrosis. Circulating levels of IL-10 and TNFα were significantly elevated post injury, indicating toll-like receptor (TLR) signaling may be involved in muscle injury. Administration of hydroxychloroquine (HCQ), a small molecule inhibitor of TLR7/8/9, following injury reduced NET formation, IL-10, and TNFα levels and ultimately mitigated muscle fibrosis and improved myofiber regeneration following IR injury. HCQ treatment decreased fibroadipogenic progenitor cell proliferation and partially inhibited ERK1/2 phosphorylation in the injured tissue, suggesting it may act through a combination of TLR7/8/9 and ERK signaling mechanisms. We demonstrate that treatment with FDA-approved HCQ leads to decreased muscle fibrosis and increased myofiber regeneration following IR injury, suggesting short-term HCQ treatment may be a viable treatment to prevent muscle fibrosis in ischemia reperfusion and traumatic extremity injury.

Abbreviations: COX, cytochrome oxidase; Ctx, cardiotoxin; DPI, days post injury; eMHC, embryonic myosin heavy chain; ERK 1/2, extracellular signal-regulated kinases 1/2; FAP, fibroadipogenic progenitor cells; H3Cit, citrullinated histone H3; HCQ, hydroxychloroquine; IL-10, interleukin 10; IR, ischemia reperfusion; *Mapk*, mitogen-activated kinase gene MPO myeloperoxidas e; NET(s), neutrophil extracellular trap(s); PAD4, peptidylarginine deiminase 4; SDH, succinate dehydrogenase; TA, tibialis anterior; TLR, toll-like receptor; TNFα, Ttumor necrosis factor alpha; *t*-SNE, t-distributed stochastic neighbor embedding.

KEYWORDS
extracellular signal-regulated kinases (ERK) 1/2, hydroxychloroquine, inflammation, muscle fibrosis

1 | INTRODUCTION

Ischemia reperfusion (IR) tissue injury can occur after any situation in which the blood supply to a tissue is profoundly interrupted resulting in microcirculatory hypo-perfusion and hypoxia. Anaerobic metabolism leads to accumulation of lactic acid, decrease of pH in tissues (metabolic acidosis), mitochondrial dysfunction, vasoactive agents, generation of reactive oxygen species, oxidative stress, endothelial activation, aberrant local inflammatory responses, organelle damage, and ultimately cell death.[1,2] Ischemia reperfusion injury occurs clinically both in controlled surgical settings such as organ transplantation and free flap procedures as well as during traumatic events, such as battlefield blast injuries involving emergency tourniquet usage to control hemorrhage. In the skeletal muscle, IR injury translates into inflammation, tissue edema, muscle fibrosis, and/or necrosis, ultimately leading to decreased range of motion or complete loss of function.[3] Therefore, determining the precise mechanism by which IR injury occurs and discover treatments to minimize the long-term consequences is of utmost importance.

The resultant tissue damage occurs secondary to tissue hypoxia and paradoxically from the reperfusion of reoxygenated blood into the ischemic tissue often referred to as hypoxic re-oxygenation injury.[2,4] One cause of IR induced tissue injury is due to an excessive innate local and systemic inflammatory immune response. Perfused leukocytes encounter released intercellular damage-associated molecular patterns (DAMPs), adhesion molecules, chemokines, glycosaminoglycans (GAGs), metalloproteinase, and extracellular calcium and adenosine triphosphate (ATP) released by necrotic cells, which induce the activation of many toll-like receptor (TLR) pathways to promote an inflammatory response.[1,5-7] Neutrophils comprise a substantial portion of the amplifier cell population in the initial immune response, and their involvement in IR injury is hypothesized to be, in part, due to the formation of neutrophil extracellular traps (NETs) containing web-like extrusions of nuclear DNA, citrullinated histones, and antimicrobial peptides released into the tissue by activated neutrophils.[8-10] NETs have been implicated in a wide variety of diseases, notably autoimmune diseases such as lupus[11-13] and rheumatoid arthritis.[14,15] Additionally, NETs have also been shown to form following traumatic injury both systemically and at the site of injury,[16-21] including in models of ischemic injury in vital organs.[5,6,18,22]

NETs have been shown to form through several other independent pathways in addition to the well-characterized peptidylarginine deiminase 4 (PAD4)-dependent pathway.[23] Recent reports suggest that NET formation also occurs when DNA and RNA stimulate toll-like receptors (TLR) on polymorphonuclear neutrophils in a process termed self-propagation or secondary NETosis.[17,24] TLR 7/8 and 9 are pattern recognition receptors expressed on cells of the innate immune system, which are classically believed to recognize pathogenic RNA and DNA, respectively. However, growing evidence suggests that aberrant activation of these TLRs with self DNA and/or RNA occur when free nucleic material is present in the tissue, such as in autoimmune diseases, viral infections, and following traumatic injuries.[17,25-31]

Small molecule inhibitors of TLR7/8/9, such as hydroxychloroquine (HCQ, Plaquenil®), were developed initially as anti-malarial agents, but have shown to be efficacious for treating lupus, an autoimmune disease characterized by excess and impaired degradation of NETs.[13,24,32-34] HCQ has also been shown to be an effective antiviral agent against RNA viruses including dengue virus and retroviruses[35] by de-acidifying endosomes required for endosome-mediated viral entry during TLR7/8/9 activation.

Ischemia reperfusion injury also leads to abnormal expression of extracellular signal-regulated kinase 1/2 (ERK1/2), however, the precise role of ERK1/2 signaling in IR injury remains controversial. Mitogen-activated protein kinase (*Mapk)* genes, such as *Mapk3* (*Erk1*) and *Mapk1* (*Erk2*), have been found to be dysregulated in multiple pathological states, including fibrotic diseases. Studies have shown inhibition of ERK1/2 signaling has been shown to attenuate fibrosis by minimizing extracellular matrix deposition in several mouse models, including hepatic IR injury[36] and kidney fibrosis.[37] Furthermore, inhibition of *Mapk* genes and decreased phosphorylation of ERK1/2 have protective effects in multiple organ systems by decreasing apoptosis and increasing cellular turnover.[38-43] In contrast, contradicting reports have shown increased activation of the same ERK pathways provide protection.[44-46] These differences suggest ERK signaling may vary depending on pathologic state/condition, thus the precise role in IR injury remains to be elucidated.

Given that excess nuclear material is observed following traumatic injury and may increase NET formation alone and through self-propagation by TLR7/8/9 signaling, we investigated the role of neutrophil signaling and NET

formation in the fibrotic response of skeletal muscle in a murine IR injury model. We next hypothesized that modulation of TLR7/8/9 using HCQ, a small molecule inhibitor to TLR7/8/9, may lead to decreased tissue injury and skeletal muscle fibrosis following IR injury by interfering with secondary self-propagated NETosis mediated by TLR7/8/9 activation. More broadly, given the role of ERK1/2 in both cellular apoptosis following IR injury and in fibrotic diseases, we also evaluated the effects of HCQ treatment on *Erk1 and Erk2* gene expression and ERK1/2 signaling following skeletal muscle IR injury. Coupling this with the known importance of neutrophils and the immune response following IR injury, we hypothesized that a combination therapy of TLR7/8/9 inhibition to target NETosis and inhibition of ERK1/2 activation would prevent skeletal muscle fibrosis following IR injury.

Here, we provide evidence that following IR injury in skeletal muscle, the initial immune response drives substantial NET formation in the injured muscle tissue that results in muscle fibrosis. We also show that HCQ treatment both inhibits proliferation of fibroadipogenic progenitor cells (FAPs), the population responsible for fibrotic deposition,[47] decreases phosphorylation of ERK1/2, and decreases NET formation. We find that administration of HCQ mitigates muscle fibrosis caused by IR injury through modulation of the initial neutrophil response, FAP proliferation, and ERK1/2 signaling.

2 | MATERIALS AND METHODS

2.1 | Animals

Male C57BL/6J mice were obtained from The Jackson Laboratory (Bar Harbor, ME, USA; stock no. 000664). PAD4$^{-/-}$ mice[48] were crossed 10 generations onto a C57BL/6 background. Matching background strains were used as controls for all transgenic experiments. All mice were 6-9 weeks of age at time of injury. Adult male (11- to 12-week-old, 350-450 g) pathogen free Sprague-Dawley rats were obtained from Taconic Biosciences (Germantown, NY, USA). Rats were housed for a minimum of 7 days for acclimatization and quarantine purposes in the vivarium located at the Walter Reed Army Institute of Research (Silver Spring, MD, USA). Animals were housed and maintained under standard conditions: 72 ± 4°F, with a 12 hours light/dark cycle and no diet restrictions. All experiments and animal care procedures were approved by the University of Michigan (mouse protocol PRO 7930) and the Naval Medical Research Center and Walter Reed Army Institute of Research (protocol 17-OUMD-31S) institutional animal care and use committees. All activities were conducted in accordance with all applicable regulations.

2.2 | Hindlimb ischemia reperfusion injury in the mouse model

Mice received pre-operative 0.06 mg/kg buprenorphine subcutaneously as an analgesic. Mice were anesthetized with 1%-3% isoflurane inhalation. A skin incision was made in the left groin and the groin fat pad was retracted to expose the femoral artery, vein, and nerve. The femoral artery and vein were separated from the nerve and an Ackland clamp was placed immediately distal to the inguinal ligament and proximal to the lateral circumflex femoral artery to induce acute hindlimb ischemia of the left lower limb. Mice remained under 2% isoflurane as left hindlimbs were subjected to 3 hours of ischemia. The clamp was removed and the hindlimb was reperfused until euthanasia at indicated time points. For mice with IR + cardiotoxin (IR + ctx) injury, 10 μL of 3 mg/mL of cardiotoxin was injected into the left tibialis anterior muscle immediately after clamp removal. Ctx (*Naja pallida,* Sigma-Aldrich, St. Louis, MO, USA; cat. no. 217503) was dissolved in sterile phosphate-buffered saline (PBS). Buprenorphine was administered at 0.06 mg/kg subcutaneously as an analgesic post-operatively and repeated at 12 and 24 hours

2.3 | Hindlimb ischemia reperfusion injury in the rat model

Rats were administered prophylactic analgesia (Buprenex, 0.05 and 1.2 mg/kg buprenorphine SR) via subcutaneous injection prior to injury and repeated at 48-72 hours, with further doses given as indicated based on animal assessment. Rats were anesthetized by intraperitoneal injection (IP; ketamine 80mg/kg and xylazine 10mg/kg). Additional boluses of ketamine and/or xylazine (10-20/1-3mg/kg) were administered to maintain a plane of general anesthesia. A pneumatic tourniquet (UDC1.6^{TM}, Hokanson, WA, USA) was used to interrupt blood flow. Limbs were elevated to reduce venous pooling and tourniquet was applied to the proximal aspect of the lower limb. The tourniquet was inflated and maintained at 280-300 mmHg pressure for 150 minutes.

2.4 | Test article preparation and dosing

Hydroxychloroquine sulfate (HCQ) (Cayman Chemical Ann Arbor, MI, USA, item no. 17911, CAS 747-36-4), was diluted to 15 mg/mL in sterile PBS and delivered via IP injection at 60 mg/kg daily, starting on the day of injury until euthanasia. A total of 100 μL of sterile PBS was delivered as the vehicle control (vehicle) via IP injection. Cl-amidine (Cayman Chemical, item no. 10599, CAS 1373232-26-8)

was diluted to 50 mg/mL in dimethylsulfoxide as a stock solution. The stock solution was diluted to 2 mg/mL in sterile PBS and 10 mg/kg Cl-amidine was delivered via IP injection daily starting on the day of injury until euthanasia. A total of 150 μL of 4% dimethylsulfoxide in sterile PBS was delivered as the vehicle control through IP injection.

2.5 | Tissue harvesting and histology/immunohistochemistry

Tibialis anterior (TA) muscles were dissected away from the bone and immediately embedded and frozen in optimal cutting temperature (OCT) compound. Contralateral uninjured TA muscles were used as uninjured control samples. Samples were stored in OCT blocks at −80°C until sectioning. Sections were cut at 7-10 μm thick on a Leica 3050S cryostat, mounted on charged slides, and stored at −80°C until analysis. Standard hematoxylin and eosin (H&E) and picrosirius red staining protocols were followed for tissue histology. For studies involving Cl-amidine treatment, 70% ethanol was used as a fixative prior to staining, for all other studies, Bouin's solution (Sigma-Aldrich, St. Louis, MO, USA) was used as a fixative. For immunofluorescent stains, samples were blocked and permeabilized with 2% serum, 1% BSA, 0.1% fish skin gelatin, 0.001% Triton X-100, and 0.0005% Tween 20. Primary antibodies (Supporting Table S1) were applied and incubated overnight at 4°C. Fluorescently conjugated secondary antibodies were added and then counterstained with Hoechst. Fluorescent samples were imaged using confocal fluorescence microscopy using a Leica SPX8 confocal microscope with 20x objective. All exposure times were optimized during initial imagining and kept constant for all subsequent imaging. Standard bright-field microscopy imaging was performed using a 4x, 20x, or 40x air objective. Appropriate primary antibody negative controls were run simultaneously with each tested sample.

2.6 | NET quantitation

Sections (10 μm) of flash frozen TA muscle were stained with antibodies for citrullinated histone H3 (H3Cit), myeloperoxidase-conjugated with FITC (MPO-FITC), and Hoechst in concentrations described in Supporting Table S1. Three high powered representative images (63x magnification) were taken in similar areas of the muscle on one muscle section per animal using a Leica SPX8 confocal microscope. The number of NETs per region of interest (ROI) were quantified by trained personnel and an average number of NETs per ROI was obtained per animal. NETs were considered colocalization of MPO-Hoechst, MPO-H3Cit-Hoechst, and/or classic web-like morphology of Hoechst and/or MPO.

2.7 | Muscle fibrosis analysis

ImageJ (National Institutes of Health, Bethesda, MD, USA) was used to calculate the percentage area of collagen based on staining with picrosirius red. The thresholding tool was used to create a mask of the area of positive staining, and this area was divided by the total area of the sample analyzed. The Huang method for thresholding was used for all images, and thresholding and analysis methods used were constant for every sample analyzed.[49] Six non-overlapping images at 40x magnification were taken on one section for each animal. The average positive staining for these images was used as the percent fibrotic area for each animal. Sections from corresponding regions of the muscle were used for every analysis.

2.8 | Cross-sectional area calculations

Tibialis anterior muscle sections (10 μm, flash frozen) were stained with Hoechst 33342, Embryonic Myosin Heavy Chain (eMHC) and laminin fluorescently labeled antibodies. Myovision muscle analysis software (University of Kentucky, Lexington, KY, USA)[50] was used to detect muscle fibers and calculate average myofiber cross-sectional area and minimum Feret diameter in three separate, non-contiguous fields of regenerating muscle at 20x magnification in four to six mice per group.

2.9 | Centralized nuclei quantitation

Tibialis anterior muscle sections (10 μm, flash frozen) were stained with hematoxylin and eosin (H&E) using standard protocols. Six non-overlapping images at 40x magnification were taken using bright-field microscopy on three sections for each animal. One section was from the proximal, middle, and distal third. Nuclei within the myofiber were identified as either central or peripheral by trained personnel. The number of myofibers in each group was divided by the total number of myofibers per image to obtain the percentage of myofibers with centralized or peripheral nuclei. The average percentage for each section was determined and used to calculate the average per animal, which is reported as % Centralized Nuclei or % Peripheral Nuclei.

2.10 | Cytochrome C oxidase/succinate dehydrogenase (COX/SDH) histochemistry and quantitation

COX/SDH staining was performed according to Ross.[51] Briefly, slides were incubated in a solution of 1X 3,3'-Diaminobenzidine (Sigma-Aldrich; cat. no. D3939),

100 μM cytochrome c (Sigma-Aldrich; cat. no. C2037) in PBS with 2 μg bovine catalase (Sigma-Aldrich; cat. no. C9322) for 40 minutes at 37°C then washed with PBS. Next, slides were incubated with 1.5 mM nitroblue tetrazolium (Sigma-Aldrich; cat. no. N6876), 130 mM sodium succinate (Sigma-Aldrich; cat. no. 818601), 0.2 mM phenazine methosulfate (Sigma-Aldrich; cat. no. P9625), and 1.0 mM sodium azide (Sigma-Aldrich; cat. no. S8032) in PBS for 40 minutes at 37°C. Slides were washed, mounted, and imaged with standard bright-field microscopy. Six non-overlapping images at 40x magnification were taken using bright-field microscopy on three sections for each animal. One section was from the proximal, middle, and distal third. To quantitate, each myofibers was classified as COX positive/negative and SDH positive/negative. The percentage of COX positive/SDH negative myofibers and COX positive/SDH positive myofibers per total myofibers was determined for each image. The average percentage for each section was determined and used to determine the average per animal, reported as proportion of myofibers COX^+/SDH^- or COX^+/SDH^+.

2.11 | PDGFRα-Ki67 staining and quantitation

Sections (10 μm) of flash frozen TA muscle were stained with antibodies for platelet derived growth factor receptor alpha (PDGFRα), Ki67, and Hoechst in concentrations described in Supporting Table S1. Three high powered representative images (63x magnification) were taken in similar areas of the muscle on three muscle sections per animal (one from each of the proximal, middle, and distal third of the muscle) using a Leica SPX8 confocal microscope. n = 4-6 animals per group. The number of cells expressing co-localized PDGFRα and Ki67 was manually identified and counted per region of interest (ROI) by trained personnel. Total PDGFRα and Ki67 quantitations were determined with ImageJ to threshold positive area with the Yen thresholding method to determine total positive staining, which is reported in pixels. A linear regression analysis was used to correlate total PDGFRα and total Ki67 staining. In order to accurately correlate the amount of PDGFRα to the corresponding Ki67 expression in the same ROI, ROIs were evaluated and plotted individually in analyses.

2.12 | Oil red O staining and quantitation

Tibialis anterior muscle sections (10 μm, flash frozen) were fixed in in 4% paraformaldehyde and stained in Oil Red O solution (3 mg/mL Oil Red O; Sigma-Aldrich; CAS 1320-06-5; in 60% isopropyl alcohol) for 15 minutes. Slides were rinsed in tap water and mounted with an aqueous mountant. Images of the entire muscle section from corresponding locations in the TA were taken at 4x magnification using bright-field microscopy. One section from the proximal, middle, and distal third of the TA were analyzed, to total three sections per animal. n = 2-5 animals per group. ImageJ was used to calculate the percentage area of positive Oil Red O staining. The image was transformed to YIQ color spectrum, the "I" spectrum was converted to an 8-bit image, and the MaxEntropy threshold was used to quantitate the area stained positively for Oil Red O. The positive area was divided by the total area of the sample to yield the % Oil Red O positive. The mean of three sections per animal was reported as one point per animal.

2.13 | Western blots

Tibialis anterior tissue was sonicated and lysed with RIPA buffer lysis system (sc-24948A, Santa Cruz Biotechnology, Dallas, TX, USA) and exposed to three freeze-thaw cycles. Samples were assessed for total protein using Pierce BCA Protein Assay Kit (Thermo Fisher Scientific, cat no. 23225). Proteins from lysate were separated in NuPAGE 4%-12% bis-tris gel (Thermo Fisher Scientific, cat no. NP0335BOX) with NuPAGE SDS running buffer (Thermo Fisher Scientific, cat no. NP0001). Protein was transferred to PVDF membrane (Thermo Fisher Scientific, cat no. IPVH00010) in NuPAGE transfer buffer (Thermo Fisher Scientific, cat no. NP0006). Membrane was washed in wash buffer (1x Tris-buffered saline-0.05% Tween-20) and blocked for 1 hours at room temperature with 5% milk protein in wash buffer. Membranes were incubated with primary antibody (Supporting Table S1) diluted in 5% BSA in wash buffer. Appropriate HRP-linked secondary was diluted in block solution. Membranes were developed and ImageJ software was used for quantitation.

2.14 | Cytokine assays

For mouse cytokine analysis, blood samples were collected at 3 days post injury (DPI) in EDTA tubes from mice treated with vehicle or HCQ (n = 3/group). Plasma was stored at −80°C until analysis without additional freeze-thaw cycles. On the day of assay, samples were diluted 1:1 with PBS and assessed using a mouse multi-spot 96-well 10-plex pro-inflammatory assay kit for mice (Mesoscale Diagnostics, Rockville, MD, USA) according to the manufacturer's guidelines. Plates were read and analyzed using the MSD Sector S600 Instrument and MSD Workbench Software version 4.0 (Mesoscale Diagnostics). A standard curve was generated to determine analyte concentration. For rat cytokine analysis, cytokine expression included here was determined in serum samples within a multiplex assay. Bio-Plex Pro™ Rat Cytokine 23-Plex assays (Bio-Rad Laboratories, Inc, Hercules, CA, USA;

cat# 12005641,) were performed on a Bio-Plex 200 Luminex system with high throughput fluidics (Bio-Rad Laboratories, Inc, cat# 171000205) which had undergone both validation (Bio-Plex Validation Kit 4.0, Bio-Rad Laboratories, Inc) and daily calibration prior to use (Bio-Plex Calibration Kit, Bio-Rad Laboratories, Inc) to standardize signal output and sensitivity between runs. Assay working ranges were determined using Bio-Plex Manager 6.1software (Bio-Rad Laboratories, Inc) and used for the automatic identification and removal of outliers and optimization of 5-PL standard curves to interpolate the concentrations of analytes in the unknown samples.

2.15 | RNA isolation and QRT-PCR

Tibialis anterior muscles were harvested at 7 days post IR injury from mice treated with vehicle or HCQ (n = 3/group). Samples were flash frozen and stored at −80°C. Total RNA was isolated using ceramic bead homogenization and the RNeasy mini kit (Qiagen, Venlo, Netherlands). First strand cDNA was generated from 1 μg total RNA using the iScriptAdvanced cDNA synthesis kit (Bio-Rad, Hercules, CA, USA). A custom low-density quantitative reverse transcription polymerase chain reaction array (qRT-PCR; Bio-Rad) containing primer sets and assay controls was designed to assess specific targets related to IR injury. The QuantStudio 7 Flex Real-Time PCR system (Thermo Fisher Scientific) was used to run the custom arrays. Gene expression levels were calculated as normalized expression relative to housekeeping gene (*Rplp0*; dCt) or fold change gene expression (normalized value relative to vehicle treatment value; ddCt).

2.16 | Single-cell RNA sequencing using 10x genomics

Single-cell tissue preparation and analysis was performed as previously described.[52] Briefly, baseline uninjured muscle (Day 0) and post-surgery Day 3 TA muscles were harvested from six IR + ctx mice and eight uninjured C57BL/6 mice. Three lanes of IR + ctx (n = 2 pooled mice per lane) and two lanes of uninjured (n = 4 pooled mice per lane) was used to maximize cell return. Harvested TAs were digested under agitation in 0.3% Type 1 Collagenase and 0.4% Dispase II (Life Technologies, Carlsbad, CA, USA. cat no 17100017 and 17105041) in RPMI 1640 medium for 45 minutes at 37°C. Cells were filtered, washed, and resuspended at ~1000 cells/μL. Cell viability was assessed and only samples with 85% or greater viability were used for sequencing. Single-cell 39 library generation was performed on the 10x Genomics Chromium Controller following the manufacturer's protocol for the v2 reagent kit (10x Genomics, Pleasanton, CA, USA). Single-cell gel bead bead-in-emulsions (GEMs) were generated, reverse transcription was performed, and the Post GEM-RT product was cleaned using DynaBeads MyOne Silane beads (Thermo Fisher Scientific). cDNA was amplified, quantified, and enzymatically fragmented and size selected for optimization using SPRIselect beads (Beckman Coulter, Brea, CA, USA). Double-sided SPRI bead cleanup was performed after end repair and A-tailing, and single-sided cleanup is done after adapter ligation. Indexes were added during PCR amplification, and a final double-sided SPRI cleanup was performed. During PCR amplification, indexes were added and double-sided SPRI was performed for final cleanup. Libraries were quantified by Kapa qPCR for Illumina Adapters (Roche) and size was determined by Agilent tapestation D1000 tapes. Read 1 primer sequence are added to the molecules during GEM incubation. P5, P7, and sample index and read 2 primer sequence are added during library construction via end repair, A-tailing, adaptor ligation, and PCR. Libraries were generated and sequenced on a HiSeq 4000 on a HiSeq 4000, (Illumina, San Diego, CA, USA) using a HiSeq 4000 PE Cluster Kit (PN PE-410-1001) with HiSeq 4000 SBS Kit (100 cycles, PN FC-410-1002) following manufacturer recommended protocols. Cell Ranger Single-Cell Software Suite 1.3 (10x Genomics, Pleasanton, CA, USA) was used to perform sample de-multiplexing, barcode processing, and single-cell gene counting (alignment, barcoding, and unique molecular identifier (UMI) count) at the University of Michigan Biomedical Core Facilities DNA Sequencing Core.[52]

2.17 | Bioinformatics analysis of single-cell RNA sequencing data

Analysis was performed as previously described.[52] Briefly, a total of ~200 million reads were generated from the 10x Genomics sequencing analysis for each of the replicates. The sequencing data were first preprocessed using the 10x Genomics software Cell Ranger and aligned to mm10 genome (GEO accession: GSE144270). Quality control and analysis was performed as previously described.[52] Downstream analysis steps were performed using Seurat pipeline[53] and included normalization, scaling, dimensionality reduction (principal component analysis [PCA], and t-distributed stochastic neighbor embedding [t-SNE]), unsupervised clustering, cluster consolidation via centroid rank correlation analysis, discovery of differentially expressed cluster specific markers, and marker enrichment. Presence of replicate batch effect was excluded by visual inspection of the contribution of each replicate to the PCA and t-SNE projections of the group. Provisional clusters were assigned via unsupervised clustering (Seurat FindClusters, Louvain algorithm, k = 30, resolution = 0.4), resulting in 21 and 17 provisional clusters for the case and control group, respectively. Provisional clusters were aligned according to the

rank correlation of their centroids, measured on the gene set derived from the intersection of the genes for each set. Final clusters were obtained by grouping similar clusters based on centroid rank correlation analysis. Clusters appear to be well distinguished in the PCA and t-SNE projections.[52] Characteristic gene expression and cluster name abbreviation key is provided in Supporting Table S2 and previously published data by Stepien et al.[52]

2.18 | Statistical analysis

Statistical tests were performed using GraphPad Prism 7.0 (GraphPad Software Inc, San Diego, CA, USA) software. Histological quantitation of stained images were subjected to Student *t* test or ANOVA with multiple comparisons post-test. Cross-sectional area and Feret diameter were represented as frequency of distribution graphed in percent frequency and compared using Komolgorov-Smirnov analysis. All data are presented as mean values with standard deviation (SD), and *P* values <.05 were considered to be statistically significant.

3 | RESULTS

3.1 | Ischemia reperfusion injury resulted in fibrosis and NET formation in the skeletal muscle

To recapitulate skeletal muscle fibrosis following IR injury, muscle injury, and fibrosis were investigated in the injured tibialis anterior muscle and contralateral healthy control of C57BL/6 mice. Skeletal muscle injury was characterized by intense leukocyte infiltration at 3 DPI with lingering necrotic myofibers as indicated by H&E staining (Supporting Figure S1). At 3 DPI, picrosirius red staining revealed loose, disorganized collagen deposition (Supporting Figure S1) and by 7 DPI, strong collagen deposition was present between regenerating myofibers, a pattern consistent with fibrotic deposition (Figure 1, Supporting Figure S1). By 7 DPI, necrotic tissue was replaced by regenerating skeletal muscle myofibers with prominent centralized nuclei, cytoplasmic basophilia, and oblong shape with smooth edges (Figure 1, Supporting Figure S1). Ischemia reperfusion injury in the skeletal muscle was also characterized by a robust immune system response. To evaluate the formation of NETs in the skeletal muscle following IR injury, muscle sections at 1 and 3 DPI were immunofluorescently labeled with H3Cit, MPO, and Hoechst and NETs were identified. Robust NET formation was demonstrated in the skeletal muscle following IR injury (Figure 1, Supporting Figure S2, indicated by white arrowheads). Neutrophil extracellular traps were not present in uninjured skeletal muscle, as shown in Supporting Figure S2.

3.2 | Decrease of NETosis via PAD4 pathway did not alter muscle regeneration or fibrosis

Protein arginine deiminase 4 (PAD4) is required for NETosis that occurs through citrullination of histone H3 and H4.[48,54-57] NETs formed in the muscle in the mouse model of IR demonstrate citrullination of histone H3 (Supporting Figure S2), thus $PAD4^{-/-}$ mice and the small molecule PAD inhibitor Cl-amidine were utilized to investigate the role of NETs formed via the PAD4 pathway in fibrotic deposition from IR injury. C57BL/6 mice underwent IR injury and were administered Cl-amidine or vehicle treatment via IP injection daily. Tibialis anterior muscles were harvested at 3 and 7 DPI, flash frozen, cryosectioned, and histologically processed to evaluate NET formation, myofiber regeneration, and muscle fibrosis. Neutrophil extracellular trap formation was quantified at 3 DPI. Daily administration of Cl-amidine led to a significant decrease in NET formation from 24.1 ± 11.7 to 3.9 ± 2.7 following treatment (NETs per 63x ROI, n = 3 per group; $P < .05$; Figure 1A). Mice treated with Cl-amidine presented with an increased frequency of myofibers with small CSA and Feret diameter ($P < .0001$, both analyses), indicating that administration of Cl-amidine hindered muscle regeneration at 7 DPI compared to vehicle (Figure 1B). Similarly, Cl-amidine did not have an effect on muscle fibrosis at 7 DPI compared to the vehicle (17.5 ± 0.41%; vs 50.6% ± 5.5% vs 47.7% ± 11.1 uninjured, Cl-amidine, vehicle, respectively; mean ± SD $P = .8$, n = 3-6/group; ordinary one-way ANOVA plus Tukey's test). (Figure 1C). As pharmacological intervention may not completely inhibit the PAD4 signaling, we next sought to investigate this phenomenon in a transgenic mouse lacking PAD4. To ensure a robust injury and closely mimic the polytrauma injuries that often accompany IR, in the complimentary transgenic studies IR injury was performed as described and 10 μL of 3 mg/mL ctx was also injected into the injured tibialis anterior immediately following clamp release. Results in the $PAD4^{-/-}$ mice were similar to that of the pharmacological inhibition. Muscle regeneration in the $PAD4^{-/-}$ mouse was decreased compared to the wild-type control, as evidenced by an increased relative frequency of myofibers with small Feret diameter ($P < .0001$; Figure 1D). Muscle fibrosis was also similar between the $PAD4^{-/-}$ mice and wild-type C57BL/6 control mice at 7 DPI (35.0% ± 4.25% vs 39.8% ± 6.7; $PAD4^{-/-}$, C57BL/6 wild-type control, respectively, mean ± SD, $P = .34$, unpaired t-test, Figure 1E). Despite a decrease in NET formation, mice treated with Cl-amidine did not have a significant difference in myofiber regeneration, as assessed by myofiber CSA and Feret diameter. To identify if any treatments or genotypes provided protective effects on the myofibers, we compared the percent of myofibers possessing centralized nuclei (indicating regenerating myofibers) between groups and the percent of myofibers exhibiting nuclei on the periphery of the myofiber (indicating an uninjured/protected myofiber). We found similar

composition between vehicle and Cl-amidine treatment (regenerating: 0.05% ± 0.08% vs 99.7% ± 0.24% vs 99.7% ± 0.14; and uninjured/protected: 99.95 ± 0.082% vs 0.35% ± 0.24% vs 0.28% ± 0.14%; uninjured, Cl-amidine, vehicle, respectively, n = 3-6/group, ANOVA followed by Tukey's test), as shown in Figure 1F. Similarly, both C57BL/6 and PAD4$^{-/-}$ muscles were comprised of nearly 100% regenerating fibers without substantial peripherally located nuclei (Figure 1G). This data indicated that PAD4 inhibition both pharmacologically and genetically did not affect the initial injury to the TA muscle or provide protective benefits to the myofibers. All these findings taken together suggest that NET formation via the PAD4

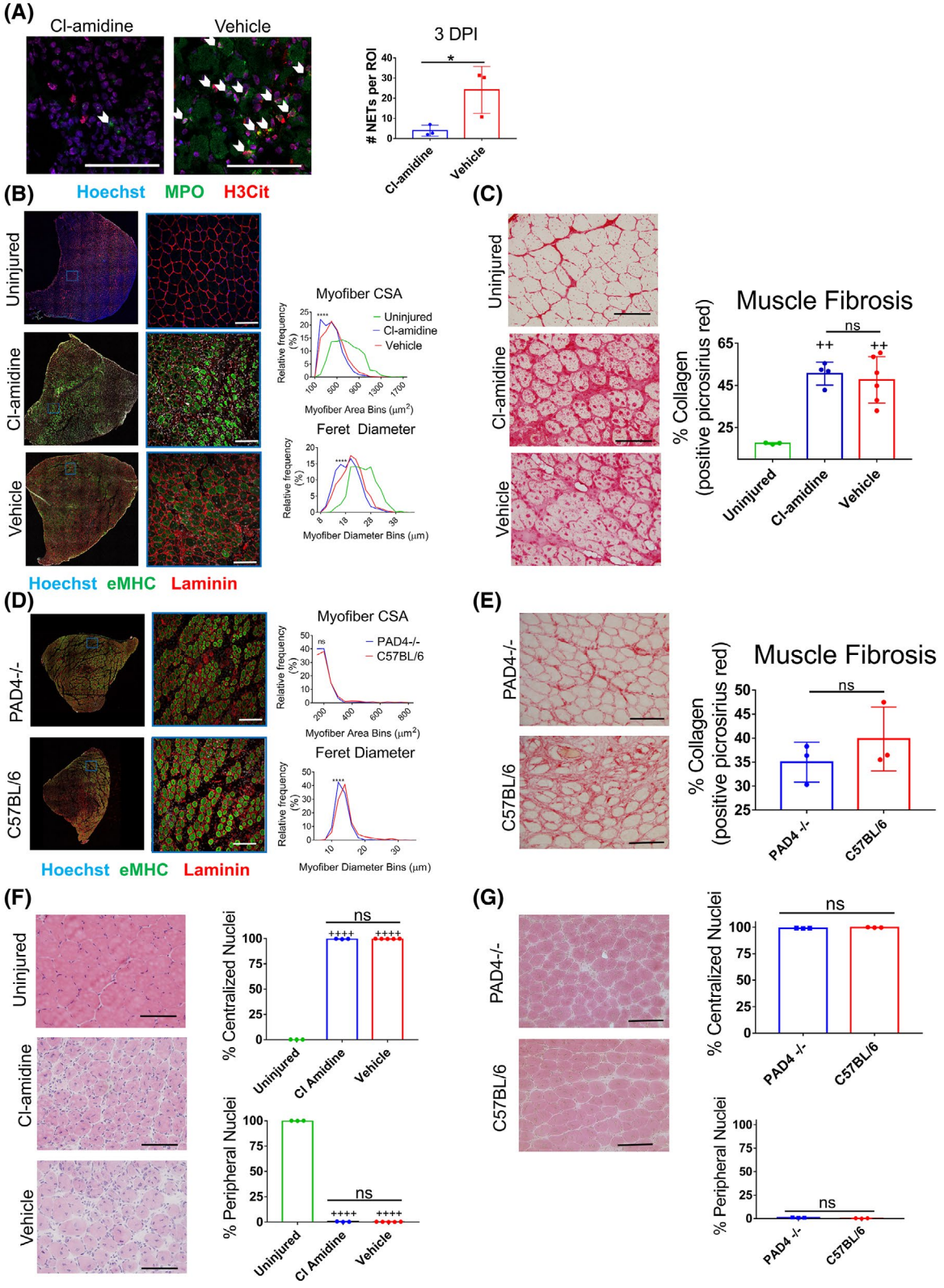

FIGURE 1 Muscle fibrosis is independent of PAD4 mediated NETosis. A, Immunofluorescent staining showing NETs (examples indicated by white arrowheads) in the tibialis anterior (TA) muscle at 3 DPI in C57BL/6 mice treated with Cl-amidine or vehicle. Treatment with Cl-amidine significantly decreased NET formation. B, Representative images of C57BL/6 mice uninjured TA, and treated with Cl-amidine or vehicle stained with eMHC and laminin at 7 DPI. Histogram of frequencies of distribution of myofiber cross sectional area (CSA) and Feret diameter at 7 DPI, indicating muscles with Cl-amidine treatment have significantly increased frequency of smaller myofibers as indicated by CSA or diameter on x-axis. C, Representative histological sections of picrosirius red staining at 7 DPI of C57BL/6 mice uninjured TA, and treated with Cl-amidine or vehicle. ImageJ quantitation of positive picrosirius red staining in the same groups. D, Representative sections of PAD4$^{-/-}$ mice or C57BL/6 wild-type control injured with IR + ctx stained with eMHC and laminin at 7 DPI. Histogram of frequencies of distribution of myofiber CSA and Feret diameter at 7 DPI, indicating PAD4$^{-/-}$ muscles have significantly increased frequency of smaller diameter myofibers. E, Representative histological sections of picrosirius red staining at 7 DPI of PAD4 $^{-/-}$ or C57BL/6 wild-type control injured with IR + ctx. ImageJ quantitation of positive picrosirius red staining in the same groups. F, Representative images of H&E stained TA 7 DPI of uninjured and treated with Cl-amidine or vehicle. Quantitation of percentage of total myofibers with centralized or peripheral nuclei in each group. G, Representative images of H&E stained muscle 7 DPI of PAD4$^{-/-}$ and C57BL/6 mice. Quantitation of percentage of total myofibers with centralized or peripheral nuclei in each group. $^{+}$Difference compared to uninjured group. All scale bars indicate 100 μm. *$P < .05$; $^{++}P < .005$; **** and $^{++++}P < .0001$. ns, not significant. Frequency distributions analyzed with Kolmogorov-Smirnov test. Bars represent means ± standard deviation. Each point represents one animal

mechanism was not essential in fibrotic deposition in the skeletal muscle following IR injury.

3.3 | IR injury induced IL-10 and TNFα production

Neutrophil extracellular traps and TLR7/8/9 have been linked to secondary self-NET propagation and have been shown to augment circulating levels of pro-inflammatory cytokines IL-10 and tumor necrosis factor-α (TNFα).[32,58] In our rat model of hind limb tourniquet-induced IR injury,[59,60] we show that IL-10 levels were significantly elevated at 6 and 24 hours post injury from 758 ± 244 pg/mL in uninjured animals to 1753 ± 121 pg/mL at 6 hours ($P < .0001$) and 1659 ± 213 pg/mL at 24 hours ($P < .0001$) (Figure 2A). We found similar elevations in TNFα at 6 and 24 hours post injury from 2633 ± 1062 pg/mL to 7047 ± 1202 pg/mL ($P < .0001$) and 6717 ± 1183 pg/mL ($P < .0001$), respectively (Figure 2A), suggesting that IR injury mimicked other NET-related disease cytokine release, and similar TLR7/8/9 mediated pathways may have also been involved. To understand the cell populations that were involved in TLR7/8/9, IL-10 and TNFα release, we conducted a transcriptome analysis of the cell types at 3 DPI involved in skeletal muscle regeneration using single-cell sequencing (scRNA-seq) in a mouse model of polytrauma (IR + ctx), which has been shown to produce a robust inflammatory reaction that results in ECM deposition, myonecrosis, and ultimately fibrosis.[52] Unsupervised clustering identified 11 distinct cellular clusters in uninjured muscle and 8 in IR + ctx (Figure 2B,C, Supporting Table S2). Uninjured muscle was largely composed of endothelial cells/vascular progenitor cells, FAPs, satellite cells, and *scleraxis* expressing mesenchymal stem cells. Injured muscle also contained an FAP population, as well as a greater predominance of immune cells including macrophages, dendritic cells, and granulocytes. Of note, the uninjured muscle was found to contain a *Pax7* positive satellite cell population, indicating quiescent satellite cells, while the injured muscle contained a myoblast population, defined by *Myf5* and *Myod1*. *Il10* was expressed nearly exclusively by the macrophage population (Figure 2D,E) and *Tnfα* at highest levels in the granulocyte population (Figure 2F,G). These results indicate that traumatic injury induced *Il10* and *Tnfα* gene expression at the same time point as robust NET formation and that NETs present in the tissue following injury may stimulate TLR7/8/9 pathways, leading to increased IL10 and TNFα levels observed here.

3.4 | Treatment with HCQ suppressed IL-10 and TNFα production

We next sought to modulate TLR signaling pathway to mitigate injury caused by IR. HCQ has been shown effective in NET and RNA mediated diseases and viral infections, and is known to lower IL-10 and TNFα levels in lupus patients as well as decrease disease severity.[61] Ischemia reperfusion injured C57BL/6 mice treated systemically with 60 mg/kg HCQ daily had a trend toward lower IL-10 and significantly lower TNFα ($P < .05$) plasma levels (Figure 2H-I) at 3 DPI, which correlates with the detected robust NET formation and presence of *Il10* and *TNFα* expressing immune cells (Figures 1A and 3C-G). Interestingly, no significant differences in other measured pro-inflammatory cytokine were detected (Supporting Table S3).

3.5 | HCQ treatment decreased NET formation

Given that HCQ acts on TLR7/8/9, we evaluated NET formation at 3 DPI in C57BL/6 mice treated with vehicle or HCQ. Mice treated with HCQ showed substantial trend toward decreased NET formation, (NETs per 63x ROI: HCQ: 4.5 ± 1.6, vehicle: 7.4 ± 3.2; n = 6/group; $P = .08$, unpaired t test) (Figure 3A). This potential decrease in NET formation in the HCQ-treated mice is unlikely to be due to differences in initial

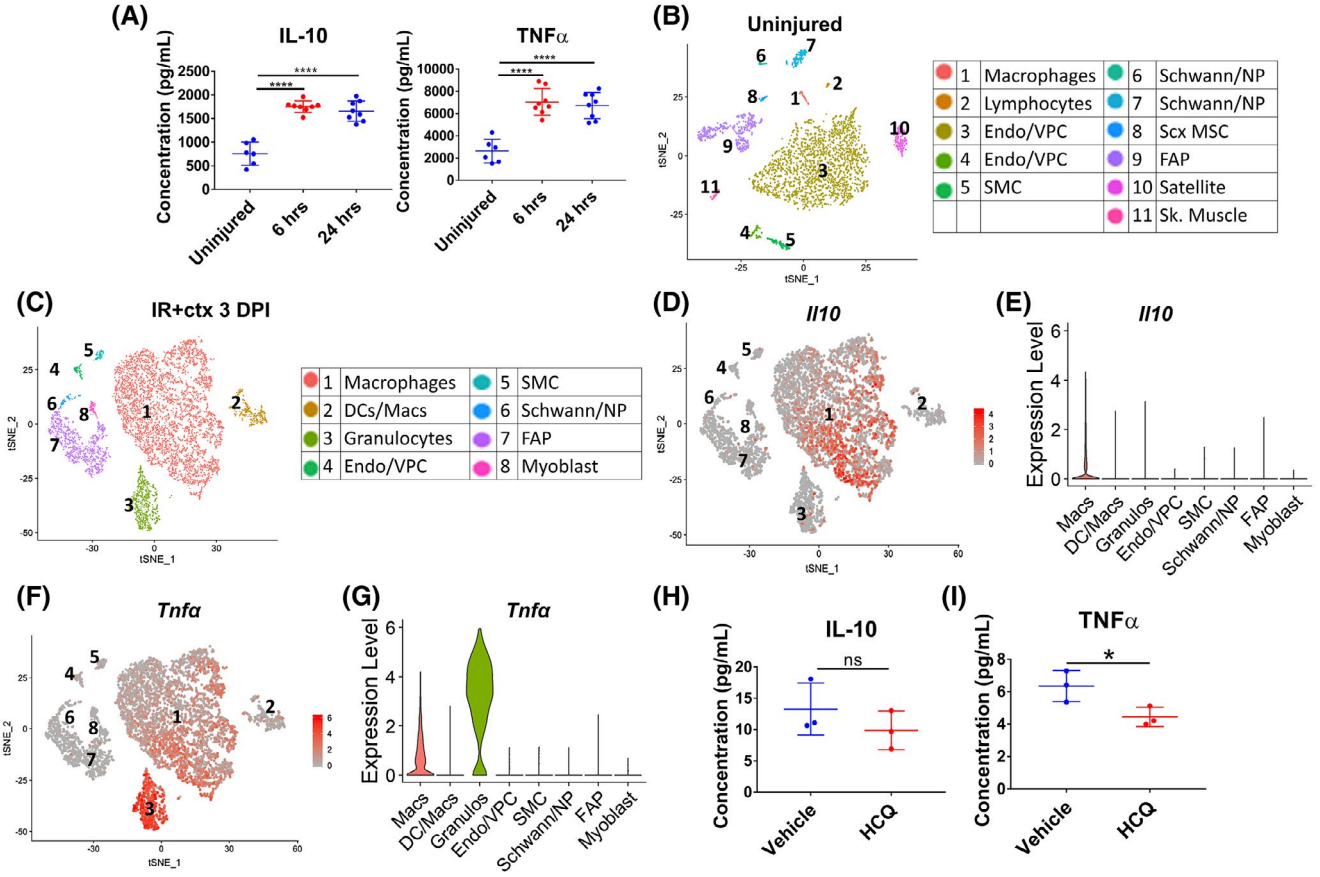

FIGURE 2 HCQ decreases IL-10 and TNFα in an IR injury model. A, In a rat model of tourniquet-induced hind limb IR injury, serum levels of IL-10 and TNFα are significantly elevated at 6 and 24 h post injury compared to uninjured levels (n = 6-8/group, one-way ANOVA with Tukey test). B, Clusters resulting from unsupervised clustering in mouse uninjured tibialis anterior muscle, overlaid letters correspond to adjacent table to indicate cluster identification. C, Clusters resulting from unsupervised clustering in mouse IR + ctx injured muscle at 3 DPI, overlaid letters correspond to adjacent table to indicate cluster identification. Violin plots indicate distribution of expression between clusters of cells at 3 DPI of (D-E) *Il10* and (F-G) *Tnfα*. HCQ lowers circulating (H) IL-10 and (I) TNFα levels at 3 DPI in the C57BL/6 mouse model of IR injury (n = 3 per group, unpaired t-test). *$P < .05$, ****$P < .0001$. Each point represents one animal

neutrophil recruitment, as treatment with HCQ did not show a difference in neutrophil recruitment to the injured muscle at 3 DPI, as assessed by immunofluorescent staining for Ly6G (Supporting Figure S3). This trend of decreased NET formation following administration of TLR7/8/9 inhibitor further indicated that NET formation is likely partially, but not completely, mediated by TLR signaling following traumatic injury.

3.6 | Treatment with HCQ attenuated fibrosis and improved myofiber regeneration following IR injury

Given the trend toward decreased NET formation observed following HCQ administration, we next sought to investigate the role of HCQ in muscle regeneration and fibrosis after IR injury. C57BL/6 mice underwent IR injury and were treated with vehicle or HCQ. Mice treated with HCQ presented with significantly decreased muscle fibrosis at 7 DPI than those treated with vehicle (18.5% ± 2.3% vs 30.4% ± 5.4% vs 40.5% ± 4.0; uninjured, HCQ, vehicle, respectively; n = 6/group, $P < .01$, ordinary one-way ANOVA plus Tukey's test) (Figure 3B). Additionally, treatment with HCQ improved muscle regeneration. HCQ decreased the frequency of myofibers with small CSA and small Feret diameters (both analyses $P < .0001$) at 5 DPI (Figure 3C). In order to determine if the differences seen in fibrosis and regeneration in the HCQ-treated animals was a result of less severe initial injury, we again compared the percentage of regenerating (centralized nuclei) and uninjured/protected (peripheral nuclei) myofibers in each treatment group to assess if HCQ provided protective effects on the myofibers. The percentage of regenerating myofibers was not significantly different between vehicle and HCQ-treated animals (0% vs 98.37% ± 2.08% vs 98.78% ± 0.49; uninjured, HCQ, vehicle, respectively, n = 6/group, ANOVA followed by Tukey's test), as shown in Figure 3D. HCQ did not prevent initial injury to the myofibers either, as the composition of peripherally located myofibers

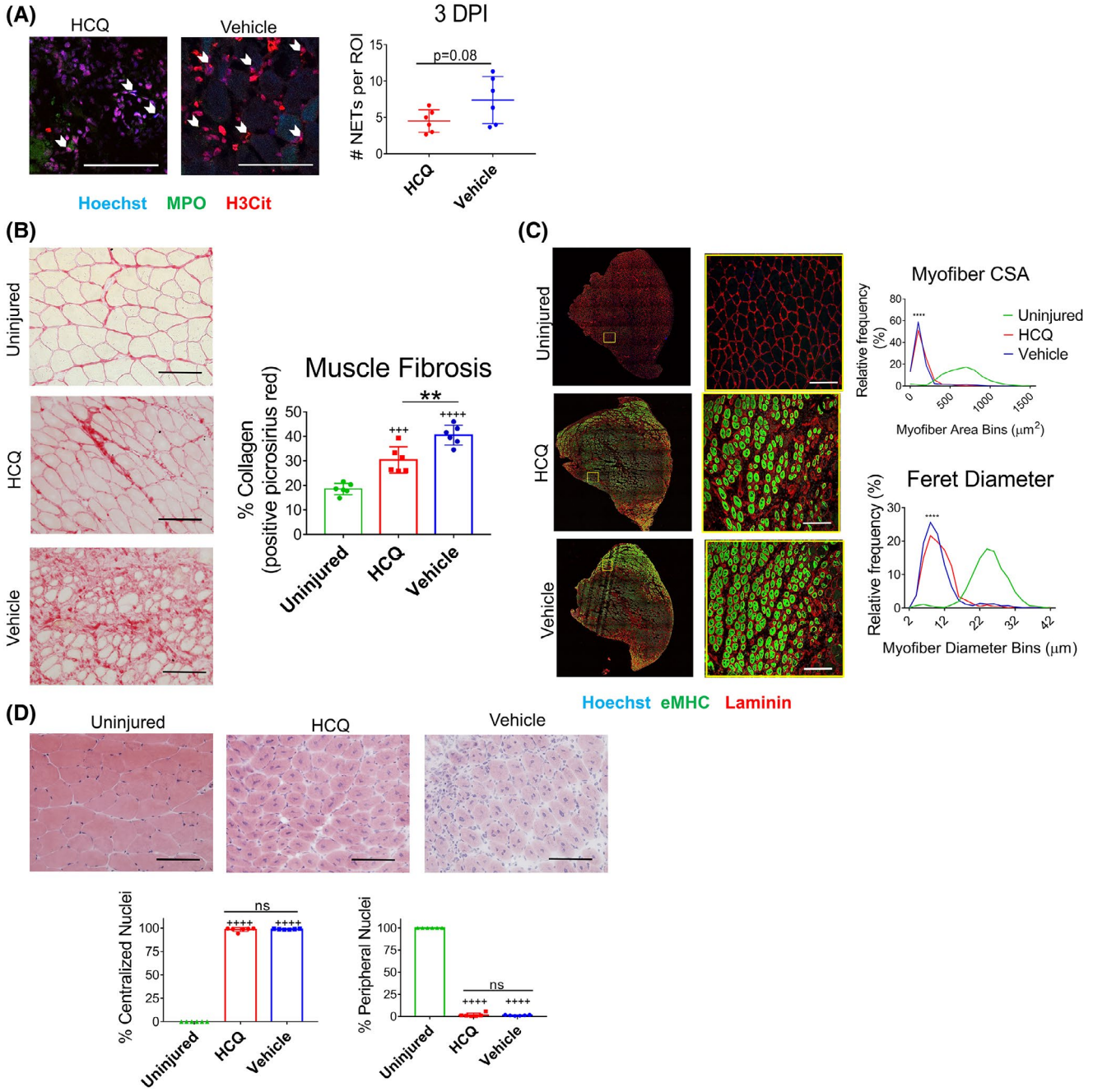

FIGURE 3 Hydroxychloroquine decreases muscle fibrosis following IR injury. A, Immunofluorescent staining showing NETs (examples indicated by white arrowheads) in the tibialis anterior muscle at 3 DPI in C57BL/6 mice treated with HCQ or vehicle. Quantitation shows HCQ treatment modestly decreased NET formation. B, Representative histological sections of picrosirius red staining of TA at 7 DPI of C57BL/6 mice uninjured and treated with HCQ or vehicle. ImageJ quantitation of positive picrosirius red staining in the same groups shows HCQ treatment decreased collagen deposition. C, Representative images of C57BL/6 mice uninjured TA and treated with HCQ or vehicle stained with eMHC and laminin at 5 DPI. Histogram of frequencies of distribution of myofiber CSA and Feret diameter, indicating muscles with vehicle treatment have significantly increased frequency of small CSA and feret diameter. D, Representative images of H&E stained TA 7 DPI in uninjured and treated with HCQ or vehicle. Quantitation of percentage of total myofibers with centralized or peripheral nuclei in each group. All scale bars indicate 100 μm. $^{+}$Difference compared to uninjured group. $^{**}P < .01$; $^{++}P < .005$; **** and $^{++++}P < .0001$. ns, not significant. Frequency distributions analyzed with Kolmogorov-Smirnov test. Bars represent means ± standard deviation. Each point represents one animal

was not significantly different between vehicle and HCQ-treated animals (100% vs 1.63% ± 2.08% vs 1.21% ± 0.49; uninjured, HCQ, vehicle, respectively, n = 6/group, ANOVA followed by Tukey's test) (Figure 3D). Taken together, this data indicated that HCQ significantly decreased fibrosis and increased regeneration following muscle IR injury.

Furthermore, our data indicated that muscle fibrosis was at least in part independent of NET formation in this injury, as the increase in regeneration and reduction in fibrosis was accompanied by a non-significant decrease in NET formation.

3.7 | HCQ treatment did not induce mitochondrial damage

Antimalarial myopathy and mitochondrial abnormalities have been reported after chronic chloroquine regimens.[62] In order to assess the presence of a mitochondrial myopathy in the injured TA following HCQ treatment, COX/SDH double staining was performed. The COX/SDH stain was used to detect fibers that lacked COX activity staining, but in which positive SDH staining was present (COX^-/SDH^+), which is indicative of mitochondrial myopathies,[63,64] or fibers that are both COX and SDH positive. No myofibers were found to lack COX staining and a significant difference was not found between the proportion of COX^+/SDH^+ myofibers of muscles treated with HCQ compared to vehicle treated, as shown in Supporting Figure S4, which indicated that 7 days of daily HCQ treatment did not induce significant mitochondrial dysfunction in the injured muscles.

3.8 | HCQ treatment inhibited FAP proliferation

Fibroadipogenic progenitors proliferate following injury and differentiate into myofibroblasts, which are responsible for ECM deposition and fibrotic deposition.[47] Having shown the HCQ decreased ECM deposition and fibrosis following IR injury, we hypothesized that HCQ may be acting on FAPs. Indeed, staining for FAPs (identified by PDGFRα expression) and the proliferation marker Ki67 at 5 DPI revealed that HCQ treatment significantly decreased the proliferation in FAP cells, as shown by a decreased number of double-positive PDGFRα-Ki67 cells in the HCQ-treated muscles compared to vehicle treated (0.1 ± 0.3 vs 2.6 ± 1.6 vs 8.5 ± 4.7; uninjured, HCQ, vehicle, respectively; n = 4-6/group, $P < .0001$, ordinary one-way ANOVA plus Tukey's test) (Figure 4A-B). Furthermore, we used linear regression analysis to correlate total PDGFRα staining with total Ki67 staining and demonstrated that vehicle-treated animals showed a significant linear correlation between PDGFRα and Ki67 stains ($P = .04$, Figure 4E), which suggested that FAPs were the proliferating population. By contrast, there was poor concordance of FAP/proliferation correlation plots of the HCQ-treated animals ($P = .17$ Figure 4D), which suggested

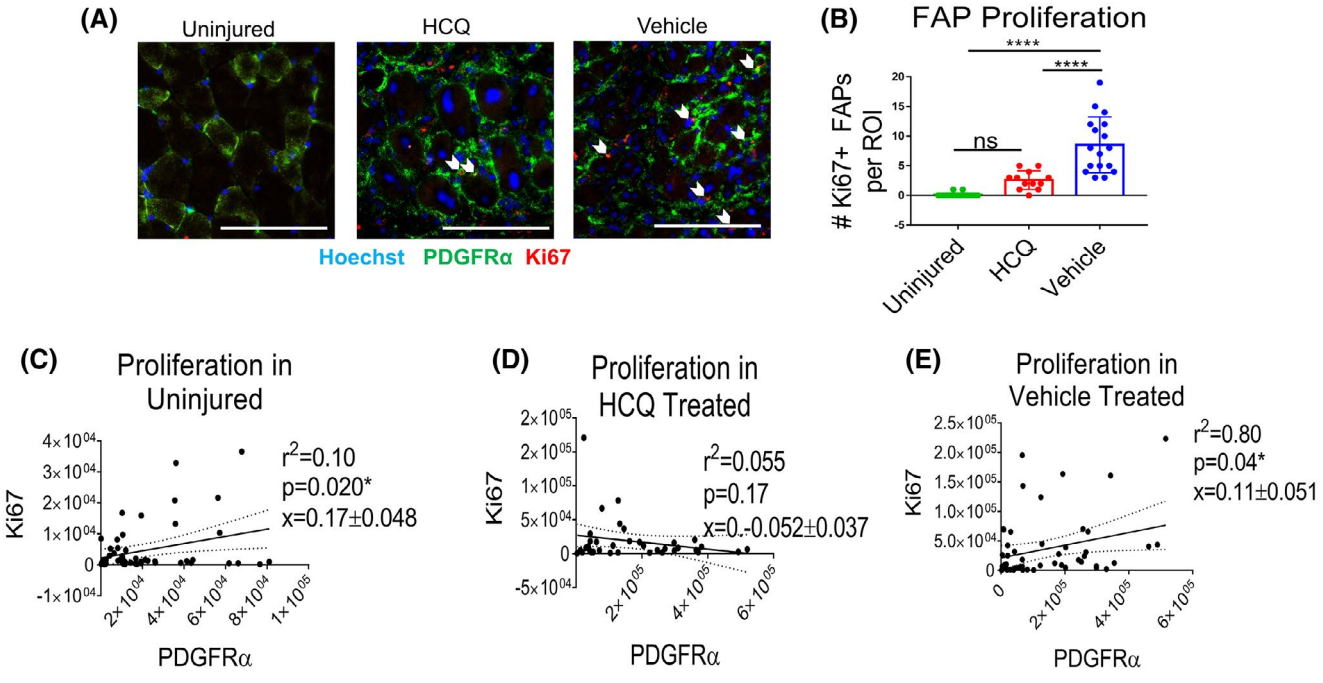

FIGURE 4 Hydroxychloroquine treatment decreases FAP proliferation. A, Immunofluorescent staining of FAPs co-stained with Ki67 (examples indicated by white arrowheads) in the TA at 5 DPI in C57BL/6 mice uninjured and treated with HCQ or vehicle. B, Quantitation of number of FAPs expressing Ki67. HCQ treatment significantly reduces the number of FAPs expressing Ki67. Correlation curves of total PDGFRα + and Ki67 + area in (C) uninjured, (D) HCQ-treated, (E) vehicle-treated tibialis anterior muscles. All scale bars indicate 100 μm *$P < .05$; ****$P < .0001$. Each point represents one ROI

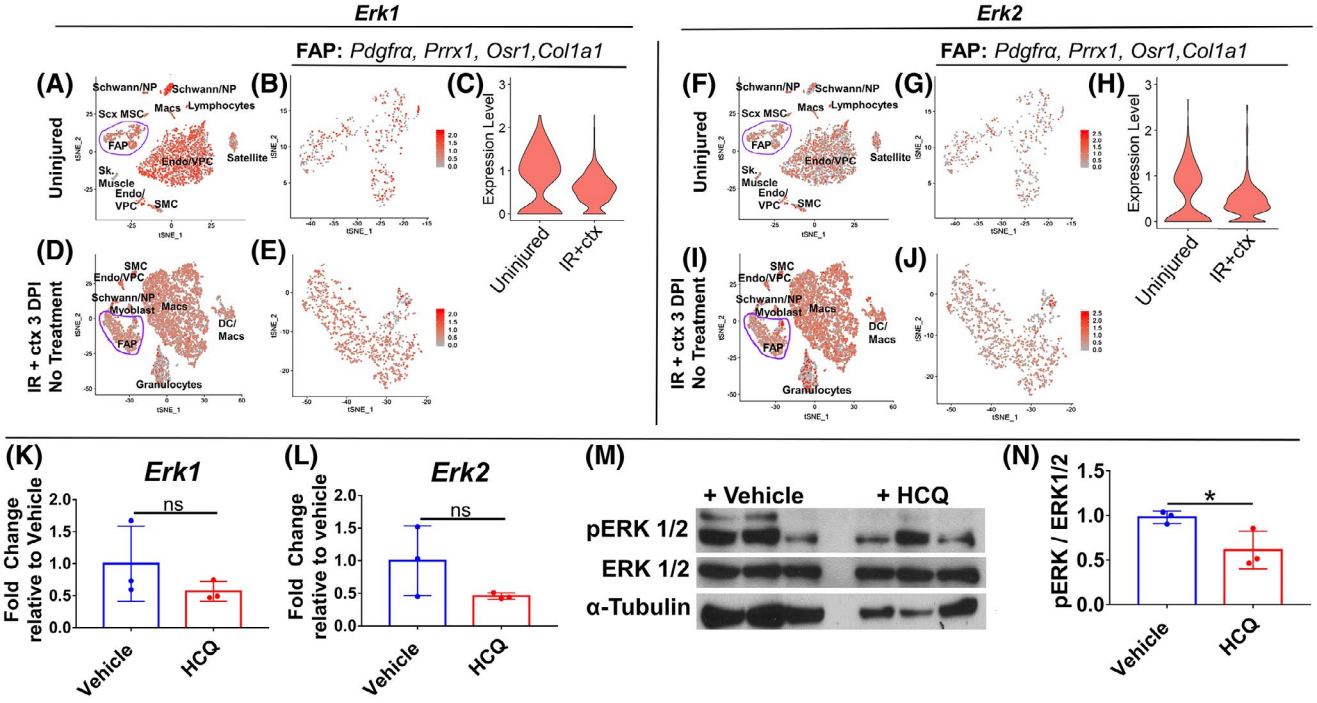

FIGURE 5 Hydroxychloroquine treatment decreases ERK1/2 phosphorylation in IR injury model. A, Single-cell RNAseq expression of *Erk1* in all cells of uninjured TA. (B) Expression of *Erk1* in FAP population of uninjured TA. C, Comparison of *Erk1* expression in FAP population of uninjured and IR + ctx FAP populations. D, Single-cell RNAseq expression of *Erk1* in all cells of IR + ctx injured TA without treatment at 3 DPI. E, Expression of *Erk1* in FAP population of IR + ctx injured tibialis anterior (TA) muscle without treatment at 3 DPI. F, Single-cell RNAseq expression of *Erk2* in all cells of uninjured TA. G, Expression of *Erk2* in FAP population of uninjured TA. H, Comparison of *Erk2* expression in FAP population of uninjured and IR + ctx FAP populations. I, Single-cell RNAseq expression of *Erk2* in all cells of IR + ctx injured TA without treatment at 3 DPI. J, Expression of *Erk2* in FAP population of IR + ctx injured TA without treatment at 3 DPI. Gene expression of (K) *Erk1* and (L) *Erk2* in the TA at 7 days post IR injury in mice treated with vehicle or HCQ. HCQ treatment does not significantly change *Erk2* or *Erk1* gene expression. Bars indicate fold change in gene expression relative to vehicle treatment. M, Western blot indicating levels of ERK1/2, phosphorylated ERK1/2 (pERK1/2), and alpha tubulin at 7 DPI in TA treated with vehicle or HCQ. N, Corresponding quantitation of pERK1/2 relative to ERK1/2 shows significant decrease in ERK1/2 phosphorylation after HCQ treatment. $^*P < .05$. Bars represent means ± standard deviation. Each point in (K-N) represents one animal

that, while Ki67 staining was present, it did not correlate to increased PDGFRα expression. Uninjured TA muscles presented with few FAPs and decreased total staining of both PDGFRα and Ki67 (Figure 4A-C). Following injury, FAPs may also differentiate to adipocytes.[47] Oil Red O staining, which identifies lipid deposition, in the vehicle and HCQ-treated TAs at 5 DPI identified very little lipid accumulation, indicating that FAPs were not driven toward adipogenesis following IR injury, nor did HCQ lead to adipocyte formation (Supporting Figure S5). Taken together, this indicated that treatment with HCQ decreased proliferation in the FAP population at 5 DPI, which corresponded to a decrease in fibrosis at 7 DPI.

3.9 | Treatment with HCQ inhibited ERK1/2 phosphorylation after IR injury

The role of ERK signaling following IR injury is not yet completely elucidated, but most studies to date show decreased ERK signaling and/or decreased ERK1/2 phosphorylation in the injured tissue to be beneficial for tissue survival and regeneration[38-43] and ERK signaling has also been implicated in fibrotic diseases.[36,37,65-67] In order to investigate the role of ERK signaling in IR injury, we analyzed the IR + ctx single-cell data set to characterize *Erk1* and *Erk2* gene expression in uninjured and injured skeletal muscle without treatment interventions. Given the central role in proliferation, transcription regulation, and differentiation, both genes were widely expressed both in the uninjured and injured muscle at 3 DPI (Figure 5A-J). Interestingly, *Erk1* and *Erk2* were differentially expressed in the FAP cell population (characteristic genes provided in Supporting Table S2 and Supporting Figure S6) after injury (Figure 5C,H). FAPs expand in response to injury and contribute to fibrotic deposition by myofibroblasts, and an increase in fibrotic gene expression (including *Col3a1, Col1a2, Snai1, Ctgf*) at this time point has previously been shown in this population.[52,68,69] A full analysis of *Erk1* and *Erk2* expression levels in each cluster of uninjured

and injured muscle is included in Supporting Figure S7. Of note, little *Erk1* or *Erk2* expression was present in the granulocyte population of the IR + ctx muscle, the population from which NETs would arise (Supporting Figure S7). Furthermore, low levels *Erk1* and *Erk2* expression was present in the satellite cell population of the uninjured satellite cell population (*Pax7*$^+$, *Chodl*$^+$, *Sdc4*$^+$), however, expression of *Erk1* and *Erk2* was present in the myoblast population (*Myod1*$^+$, *Myf5*$^+$) of the IR + ctx injured muscle at 3 DPI (Supporting Figure S7). We next investigated *Erk1* and *Erk2* expression at 7 DPI in muscles treated with vehicle or HCQ. At 7 DPI, at which point a decrease in fibrotic deposition was seen in HCQ-treated mice, *Erk1* and *Erk2* gene expression was similar in whole muscle tissue of vehicle or HCQ-treated mice (Figure 5K-L), which indicated that treatment with HCQ does not significantly change genetic expression of *Erk1* or *Erk2*. Additional genes of interest are presented in Supporting Table S4. Similarly, whole tissue protein analysis by western blot showed similar levels of ERK1/2 protein in tissues treated with vehicle or HCQ at 7 DPI (Figure 5M). However, animals treated with HCQ showed a significantly lower ratio of pERK1/2 to ERK1/2 than the vehicle-treated mice (vehicle: 0.98 ± 0.07; HCQ: 0.61 ± 0.21, n = 3/group, $P < .05$, unpaired *t* test), which indicated that treatment with HCQ decreased ERK1/2 phosphorylation in the injured muscle tissue (Figure 5M,N). Concurrently at 7 DPI, mice treated with HCQ also presented with decreased muscle fibrosis, suggesting that inhibition of ERK1/2 phosphorylation contributed to decreased muscle fibrosis. At 7 DPI, *Erk1* and *Erk2* gene expression were similar in bulk muscle treated with vehicle or HCQ, however, HCQ inhibited ERK1/2 phosphorylation in the muscle tissue, which corresponded to a decrease in muscle fibrosis.

4 | DISCUSSION

Following a period of ischemia and subsequent reperfusion, devastating fibrosis is often formed in skeletal muscle.[3] Here, we recapitulated this injury in a mouse model of hindlimb IR injury. We showed that IR injury resulted in extensive immune infiltration post injury and led to fibrotic deposition by 7 DPI. As part of the initial immune response, we identified robust NET formation in the skeletal muscle. We found that modulation of TLR7/8/9 signaling by administration of HCQ following injury lowered circulating TNFα levels, showed a trend to lower IL-10 levels, significantly improved muscle regeneration, and attenuated muscle fibrosis. This effect was at least in part independent of NET formation via TLR7/8/9 signaling as NET formation in the HCQ-treated mice was not significantly decreased. Upon further investigation, we identified that HCQ decreased proliferation in FAP cells and modulated ERK1/2 phosphorylation, a pathway known to be involved in the fibrotic response to IR injury. Administration of HCQ may be an effective treatment to mitigate muscle damage and fibrosis following IR injury.

Following IR injury, we identified extensive neutrophil infiltration into the injured muscle and robust NET formation in the injured skeletal muscle. NETs are present in other models of trauma, and are known to exacerbate the injury in many cases.[1,4,5,70] For example, following a 30% total body surface area burn in combination with an Achilles tendon tenotomy, mice exhibit robust NET formation at the tenotomy site at 3 days post injury.[17] A mouse model of antibody-mediated transfusion-related acute lung injury also shows NETs in the alveoli of injured mice, and following an experimental model of murine deep vein thrombosis in the inferior vena cava, NETs are present in the thrombus and contribute to thrombosis.[18,19] Therefore, in the current study, we investigated if NET formation following IR injury may also negatively affect tissue regeneration and contribute to fibrosis. Classically, NETs are formed through suicidal NETosis and citrullination of histone H3, a pathway dependent on PAD4. Thus, we inhibited PAD4 pharmacologically as well as deleted PAD4 genetically to investigate the role of suicidal NETosis in muscle fibrosis. While NETs were decreased after Cl-amidine treatment, interestingly, little difference was seen in fibrotic deposition after pharmacological or genetic deletion of PAD4. These results suggested that NET formation via the PAD4 mechanism did not play an essential role in fibrotic deposition in the skeletal muscle following IR injury. However, NETs have also been shown to form through a TLR 7/8/9 mediated pathway that is independent of PAD4 via secondary self-propagation.[17,24] That is, nucleic acid material present in the tissue stimulates the TLR7/8/9 receptors of immune cells, which triggers additional inflammation and a second wave of neutrophils and NETs. We have shown that NETs were abundant in the injured tissue, which may go on to contribute to secondary NETosis. Additionally, while not explicitly investigated here, it is reasonable to hypothesize that free nucleic material was present in the tissue due to mechanical trauma.[21,71] Thus, we investigated TLR7/8/9 signaling further in the context of muscle fibrosis and NET formation.

Neutrophil extracellular traps are perhaps best characterized in autoimmune diseases such as lupus and rheumatoid arthritis, and we saw several similarities between the IR injury and these diseases, despite the vastly different underlying pathologies. First, we showed that the immune response to IR injury led to elevated serum levels of IL-10 and TNFα, which are associated with TLR7/8/9 stimulation and NETs. For example, NETs formed upon activation of neutrophils with *Mycobacterium tuberculosis*, which acts through TLR7/8/9 activation, stimulate macrophages and monocytes to produce IL-10 and TNFα.[72] High serum levels of IL-10 and TNFα

are also implicated with rheumatoid arthritis and lupus, both diseases characterized by excessive NET production.[11-13,32] In fact, increased levels of IL-10 in lupus patients has been correlated to increased disease severity.[73] We found that in our mouse model of IR injury, high serum levels of IL-10, and TNFα corresponded to the time point at which NETs are present in the injured tissue (3 DPI). Using scRNA-seq in the IR + ctx model, we identified that *Il10* was expressed by the macrophage population, and *Tnfα* largely by the granulocyte population, indicating that the infiltrating immune cells were responsible for increased circulating IL-10 and TNFα levels. Interestingly, pulmonary fibrosis can be seen in lupus, and NETs are also abundant in the airway fluids of cystic fibrosis patients, further suggesting a link between NETs and fibrosis.[74] Therefore, we chose to investigate HCQ, a small molecule TLR7/8/9 inhibitor that is prescribed for lupus and rheumatoid arthritis patients and has been shown to decrease TNFα serum levels in NET-associated diseases.[75,76] Indeed, delivery of the TLR7/8/9 inhibitor HCQ to mice following IR injury lowered TNFα levels as well as IL-10. Thus, we hypothesized that administration of HCQ following IR injury may also affect NET formation and muscle injury.

We found that HCQ significantly improved muscle regeneration and decreased muscle fibrosis following IR injury, however, HCQ treatment resulted in a non-significant decrease in NET formation. HCQ is also known to inhibit TLR7/8 signaling as well as have effects on autophagy and metabolic activity, both of which may contribute to the pro-regenerative and anti-fibrotic effect seen here.[77,78] We have also shown that treatment with HCQ decreases proliferation in the FAP cell population, which differentiate to myofibroblasts and are ultimately responsible for fibrotic deposition.[47] While further studies are needed to elucidate the cell specific actions of HCQ, we hypothesize that the decrease in FAP proliferation after HCQ treatment is at least partially responsible for the concordant decrease fibrotic deposition.

A growing body of research also ties *Mapk* signaling and ERK1/2 activation to fibrosis, and inhibition of ERK1/2 is shown to attenuate fibrosis.[36,37,65-67] Here, we showed that differential *Erk1* and *Erk2* signaling in the FAP population of IR + ctx injured skeletal muscle correlated to increased fibrotic gene expression in the FAP population, which suggested a correlation between *Mapk* signaling and fibrosis.[52] Thus, we investigated the role of *Erk1* and *Erk2* gene expression and ERK1/2 protein levels and phosphorylation in IR injury. We found that administration of HCQ decreased ERK1/2 phosphorylation at 7 DPI, which corresponded to decreased fibrosis. *Erk1* and *Erk2* expression in the muscle was similar in muscle treated with HCQ or vehicle, as were the levels of ERK1/2 protein, which indicated that the activation and subsequent phosphorylation of ERK1/2 were likely the important step in the ERK signaling process directing fibrosis. Further investigation into the role of ERK1/2 activation and related pathways will be an important next step to characterize the role of HCQ treatment in muscle fibrosis.

We have identified that treatment with FDA-approved HCQ mitigated muscle fibrosis and improved myofiber regeneration following IR injury, suggesting HCQ may be a viable treatment to prevent muscle fibrosis in ischemia reperfusion and traumatic extremity injury. Although chloroquine-induced myopathy has been reported, this side effect is rare and reversible once the dosing regimen is stopped.[62,79,80] We found that daily dosing of 60 mg/kg HCQ for 7 days did not lead to mitochondrial dysfunction in the injured muscle, as assessed by COX/SDH double staining. Overall, HCQ decreased IL-10, TNFα, FAP proliferation, and ERK1/2 phosphorylation, which contributed to the pro-regenerative and anti-fibrotic effects observed. Administration of HCQ resulted in a modest decrease of NETs in the skeletal muscle, which suggested that the muscle fibrosis following IR injury was at least partially independent of NET formation. Similarly, mice with PAD4 pharmacologically inhibited or genetically deleted, and therefore lacking NETs formed via citrullination of histone H3 did not present with differences in muscle fibrosis, which suggested fibrosis is independent of NET formation via PAD4. These insights into the role of NETs in fibrotic injuries and mechanisms of HCQ may offer important therapies in addition to HCQ and contribute to understanding the role of NETs in traumatic and fibrotic injuries. Further investigation will focus on the mechanism of action of HCQ in muscle fibrosis.

ACKNOWLEDGMENTS

We acknowledge current and former members of the Levi lab at University of Michigan for thoughtful discussions. We also acknowledge: K. Kessell and members of University of Michigan and Walter Reed Army Institute of Research Unit for Laboratory Animal Medicine for excellent colony management and animal care and the University of Michigan Microscopy Core for expert advice in microscopy presented here.

CONFLICT OF INTEREST

The authors have no relevant conflict of interest.

AUTHOR CONTRIBUTIONS

N. Edwards, B. Levi designed research; N. Edwards, C. Hwang, P. Spreadborough, C. Pagani, S. Marini, C. Rowe, P. Yu, A. Mei, N. Visser performed experiments; N. Edwards, S. Marini, C. Hwang analyzed data; A. Huber, A. Strong, G. Hespe, S. Li, J. Knight, M. Shelef, T. Davis, B. Levi provided intellectual contributions and critical review; N. Edwards and B. Levi wrote the paper with input and final approval from all authors.

DISCLAIMERS

The opinions or assertions contained herein are the private ones of the authors and are not to be construed as official or reflecting the views of the Department of Defense, the Uniformed Services University of the Health Sciences or any other agency of the US Government.

REFERENCES

1. Gillani S, Cao J, Suzuki T, Hak DJ. The effect of ischemia reperfusion injury on skeletal muscle. *Injury*. 2012;43(6):670-675.
2. de Groot H, Rauen U. Ischemia-reperfusion injury: processes in pathogenetic networks: a review. *Transplant Proc*. 2007;39(2):481-484.
3. David Cholok EL, Lisiecki J, Agarwal S, et al. Traumatic muscle fibrosis: From pathway to prevention. *J Trauma Acute Care Surg*. 2016;82(1):174-184.
4. Kalogeris T, Baines CP, Krenz M, Korthuis RJ. Cell biology of ischemia/reperfusion injury. *Int Rev Cell Mol Biol*. 2012;298:229-317.
5. Oklu R, Albadawi H, Jones JE, Yoo HJ, Watkins MT. Reduced hind limb ischemia-reperfusion injury in Toll-like receptor-4 mutant mice is associated with decreased neutrophil extracellular traps. *J Vasc Surg*. 2013;58(6):1627-1636.
6. Albadawi H, Oklu R, Raacke Malley RE, et al. Effect of DNase I treatment and neutrophil depletion on acute limb ischemia-reperfusion injury in mice. *J Vasc Surg*. 2016;64(2):484-493.
7. Patel R, Albadawi H, Steudel W, et al. Inhalation of carbon monoxide reduces skeletal muscle injury after hind limb ischemia-reperfusion injury in mice. *Am J Surg*. 2012;203(4):488-495.
8. Honda M, Takeichi T, Asonuma K, Tanaka K, Kusunoki M, Inomata Y. Intravital imaging of neutrophil recruitment in hepatic ischemia-reperfusion injury in mice. *Transplantation*. 2013;95(4):551-558.
9. de Oliveira THC, Marques PE, Poosti F, et al. Intravital microscopic evaluation of the effects of a CXCR2 antagonist in a model of liver ischemia reperfusion injury in mice. *Front Immunol*. 2017;8:1917.
10. Brinkmann V, Reichard U, Goosmann C, et al. Neutrophil extracellular traps kill bacteria. *Science*. 2004;303(5663):1532-1535.
11. Knight JS, Subramanian V, O'Dell AA, et al. Peptidylarginine deiminase inhibition disrupts NET formation and protects against kidney, skin and vascular disease in lupus-prone MRL/lpr mice. *Ann Rheum Dis*. 2015;74(12):2199-2206.
12. Knight JS, Zhao W, Luo W, et al. Peptidylarginine deiminase inhibition is immunomodulatory and vasculoprotective in murine lupus. *J Clin Invest*. 2013;123(7):2981-2993.
13. Lande R, Ganguly D, Facchinetti V, et al. Neutrophils activate plasmacytoid dendritic cells by releasing self-DNA-peptide complexes in systemic lupus erythematosus. *Sci Transl Med*. 2011;3(73):73ra19.
14. Khandpur R, Carmona-Rivera C, Vivekanandan-Giri A, et al. NETs are a source of citrullinated autoantigens and stimulate inflammatory responses in rheumatoid arthritis. *Sci Transl Med*. 2013;5(178):178ra40.
15. Willis VC, Banda NK, Cordova KN, et al. Protein arginine deiminase 4 inhibition is sufficient for the amelioration of collagen-induced arthritis. *Clin Exp Immunol*. 2017;188(2):263-274.
16. Wong SL, Wagner DD. Peptidylarginine deiminase 4: a nuclear button triggering neutrophil extracellular traps in inflammatory diseases and aging. *FASEB J*. 2018;32:6358-6370.
17. Agarwal S, Loder SJ, Cholok D, et al. Disruption of neutrophil extracellular traps (NETs) links mechanical strain to post-traumatic inflammation. *Front Immunol*. 2019;10:2148.
18. Brill A, Fuchs TA, Savchenko AS, et al. Neutrophil extracellular traps promote deep vein thrombosis in mice. *J Thromb Haemost*. 2012;10(1):136-144.
19. Caudrillier A, Kessenbrock K, Gilliss BM, et al. Platelets induce neutrophil extracellular traps in transfusion-related acute lung injury. *J Clin Invest*. 2012;122(7):2661-2671.
20. Itagaki K, Kaczmarek E, Lee YT, et al. Mitochondrial DNA released by trauma induces neutrophil extracellular traps. *PLoS One*. 2015;10(3):e0120549.
21. McIlroy DJ, Jarnicki AG, Au GG, et al. Mitochondrial DNA neutrophil extracellular traps are formed after trauma and subsequent surgery. *J Crit Care*. 2014;29(6):1133.e1-1133.e5.
22. Allen C, Thornton P, Denes A, et al. Neutrophil cerebrovascular transmigration triggers rapid neurotoxicity through release of proteases associated with decondensed DNA. *J Immunol*. 2012;189(1):381-392.
23. Kenny EF, Herzig A, Kruger R, et al. Diverse stimuli engage different neutrophil extracellular trap pathways. *Elife*. 2017;6:e24437.
24. Herster F, Bittner Z, Archer NK, et al. Neutrophil extracellular trap-associated RNA and LL37 enable self-amplifying inflammation in psoriasis. *Nat Commun*. 2020;11(1):105.
25. Barton GM, Kagan JC, Medzhitov R. Intracellular localization of Toll-like receptor 9 prevents recognition of self DNA but facilitates access to viral DNA. *Nat Immunol*. 2006;7(1):49-56.
26. Carmelo Carmona-Rivera PMC, Moore E, Lingampalli N, et al. Synovial fibroblast-neutrophil interactions promote pathogenic adaptive immunity in rheumatoid arthritis. *Sci Immunol*. 2017;2(10):eaag3358.
27. Lindau D, Mussard J, Rabsteyn A, et al. TLR9 independent interferon alpha production by neutrophils on NETosis in response to circulating chromatin, a key lupus autoantigen. *Ann Rheum Dis*. 2014;73(12):2199-2207.
28. Liu L, Mao Y, Xu B, et al. Induction of neutrophil extracellular traps during tissue injury: Involvement of STING and Toll-like receptor 9 pathways. *Cell Prolif*. 2019;e12579.
29. Mallavia B, Liu F, Lefrancais E, et al. Mitochondrial DNA stimulates TLR9-dependent NET formation in primary graft dysfunction. *Am J Respir Cell Mol Biol*. 2019;62(3):364-372.
30. Nie M, Yang L, Bi X, et al. Neutrophil extracellular traps induced by IL8 promote diffuse large B-cell lymphoma progression via the TLR9 signaling. *Clin Cancer Res*. 2019;25(6):1867-1879.
31. Chowdhury CS, Giaglis S, Walker UA, Buser A, Hahn S, Hasler P. Enhanced neutrophil extracellular trap generation in rheumatoid arthritis: analysis of underlying signal transduction pathways and potential diagnostic utility. *Arthritis Res Ther*. 2014;16(R122):1-14.
32. Garcia-Romo GS, Caielli S, Vega B, et al. Netting neutrophils are major inducers of type I IFN production in pediatric systemic lupus erythematosus. *Sci Transl Med*. 2011;3(73):73ra20.
33. Hakkim A, Furnrohr BG, Amann K, et al. Impairment of neutrophil extracellular trap degradation is associated with lupus nephritis. *Proc Natl Acad Sci U S A*. 2010;107(21):9813-9818.
34. Leffler J, Ciacma K, Gullstrand B, Bengtsson AA, Martin M, Blom AM. A subset of patients with systemic lupus erythematosus fails to degrade DNA from multiple clinically relevant sources. *Arthritis Res Ther*. 2015;17:205.

35. Wang LF, Lin YS, Huang NC, et al. Hydroxychloroquine-inhibited dengue virus is associated with host defense machinery. *J Interferon Cytokine Res*. 2015;35(3):143-156.
36. Zhong W, Shen WF, Ning BF, et al. Inhibition of extracellular signal-regulated kinase 1 by adenovirus mediated small interfering RNA attenuates hepatic fibrosis in rats. *Hepatology*. 2009;50(5):1524-1536.
37. Andrikopoulos P, Kieswich J, Pacheco S, et al. The MEK inhibitor trametinib ameliorates kidney fibrosis by suppressing ERK1/2 and mTORC1 signaling. *J Am Soc Nephrol*. 2019;30(1):33-49.
38. Collier JB, Whitaker RM, Eblen ST, Schnellmann RG. Rapid renal regulation of peroxisome proliferator-activated receptor gamma coactivator-1alpha by extracellular signal-regulated kinase 1/2 in physiological and pathological conditions. *J Biol Chem*. 2016;291(52):26850-26859.
39. Okada M, Yamane M, Yamamoto S, et al. SPRED2 deficiency may lead to lung ischemia-reperfusion injury via ERK1/2 signaling pathway activation. *Surg Today*. 2018;48(12):1089-1095.
40. Zhang J, Xia J, Zhang Y, et al. HMGB1-TLR4 signaling participates in renal ischemia reperfusion injury and could be attenuated by dexamethasone-mediated inhibition of the ERK/NF-kB pathway. *Am J Transl Res*. 2016;8(10):4054-4067.
41. Zhou QL, Teng F, Zhang YS, Sun Q, Cao YX, Meng GW. FPR1 gene silencing suppresses cardiomyocyte apoptosis and ventricular remodeling in rats with ischemia/reperfusion injury through the inhibition of MAPK signaling pathway. *Exp Cell Res*. 2018;370(2):506-518.
42. Zhu BL, Xie CL, Hu NN, Zhu XB, Liu CF. Inhibiting of GRASP65 phosphorylation by DL-3-N-butylphthalide protects against cerebral ischemia-reperfusion injury via ERK signaling. *Behav Neurol*. 2018;2018:5701719.
43. Xu S, Niu P, Chen K, et al. The liver protection of propylene glycol alginate sodium sulfate preconditioning against ischemia reperfusion injury: focusing MAPK pathway activity. *Sci Rep*. 2017;7(1):15175.
44. Cai Y, Wang W, Qiu Y, et al. KGF inhibits hypoxia-induced intestinal epithelial cell apoptosis by upregulating AKT/ERK pathway-dependent E-cadherin expression. *Biomed Pharmacother*. 2018;105:1318-1324.
45. Chen Y, Ba L, Huang W, et al. Role of carvacrol in cardioprotection against myocardial ischemia/reperfusion injury in rats through activation of MAPK/ERK and Akt/eNOS signaling pathways. *Eur J Pharmacol*. 2017;796:90-100.
46. Choi DE, Jeong JY, Choi H, et al. ERK phosphorylation plays an important role in the protection afforded by hypothermia against renal ischemia-reperfusion injury. *Surgery*. 2017;161(2):444-452.
47. Uezumi A, Ito T, Morikawa D, et al. Fibrosis and adipogenesis originate from a common mesenchymal progenitor in skeletal muscle. *J Cell Sci*. 2011;124(Pt 21):3654-3664.
48. Li P, Li M, Lindberg MR, Kennett MJ, Xiong N, Wang Y. PAD4 is essential for antibacterial innate immunity mediated by neutrophil extracellular traps. *J Exp Med*. 2010;207(9):1853-1862.
49. Huang L, Wang MJ. Image thresholding by minimizing the measures of fuzziness. *Pattern Recognit*. 1995;28(1):41-51.
50. Wen Y, Murach KA, Vechetti IJ Jr, et al. MyoVision: software for automated high-content analysis of skeletal muscle immunohistochemistry. *J Appl Physiol*. 2018;124(1):40-51.
51. Ross JM. Visualization of mitochondrial respiratory function using cytochrome c oxidase/succinate dehydrogenase (COX/SDH) double-labeling histochemistry. *J Vis Exp*. 2011;57:e3266.
52. Stepien DM, Hwang C, Marini S, et al. Tuning macrophage phenotype to mitigate skeletal muscle fibrosis. *J Immunol*. 2020;204(8):2203-2215.
53. Butler A, Hoffman P, Smibert P, Papalexi E, Satija R. Integrating single-cell transcriptomic data across different conditions, technologies, and species. *Nat Biotechnol*. 2018;36(5):411-420.
54. Kusunoki Y, Nakazawa D, Shida H, et al. Peptidylarginine deiminase inhibitor suppresses neutrophil extracellular trap formation and MPO-ANCA production. *Front Immunol*. 2016;7:227.
55. Lewis HD, Liddle J, Coote JE, et al. Inhibition of PAD4 activity is sufficient to disrupt mouse and human NET formation. *Nat Chem Biol*. 2015;11(3):189-191.
56. Sorensen OE, Borregaard N. Neutrophil extracellular traps - the dark side of neutrophils. *J Clin Invest*. 2016;126(5):1612-1620.
57. Yanming Wang JW, Sayegh J, Lee Y-H, et al. Human PAD4 regulates histone arginine methylation levels via demethylimination. *Science*. 2004;306:279-283.
58. Guimaraes-Costa AB, Rochael NC, Oliveira F, Echevarria-Lima J, Saraiva EM. Neutrophil extracellular traps reprogram IL-4/GM-CSF-induced monocyte differentiation to anti-inflammatory macrophages. *Front Immunol*. 2017;8:523.
59. Kim JG, Lee J, Roe J, Tromberg BJ, Brenner M, Walters TJ. Hemodynamic changes in rat leg muscles during tourniquet-induced ischemia-reperfusion injury observed by near-infrared spectroscopy. *Physiol Meas*. 2009;30(7):529-540.
60. Walters TJ, Kragh JF, Baer DG. Influence of fiber-type composition on recovery from tourniquet-induced skeletal muscle ischemia-reperfusion injury. *Appl Physiol Nutr Metab*. 2008;33(2):272-281.
61. Willis R, Seif AM, McGwin G Jr, et al. Effect of hydroxychloroquine treatment on pro-inflammatory cytokines and disease activity in SLE patients: data from LUMINA (LXXV), a multiethnic US cohort. *Lupus*. 2012;21(8):830-835.
62. Casado E, Gratacos J, Tolosa C, et al. Antimalarial myopathy: an underdiagnosed complication? Prospective longitudinal study of 119 patients. *Ann Rheum Dis*. 2006;65(3):385-390.
63. Taylor RW, Schaefer AM, Barron MJ, McFarland R, Turnbull DM. The diagnosis of mitochondrial muscle disease. *Neuromuscul Disord*. 2004;14(4):237-245.
64. Thomas MM, Wang DC, D'Souza DM, et al. Muscle-specific AMPK beta1beta2-null mice display a myopathy due to loss of capillary density in nonpostural muscles. *FASEB J*. 2014;28(5):2098-2107.
65. Foglia B, Cannito S, Bocca C, Parola M, Novo E. ERK pathway in activated, myofibroblast-like, hepatic stellate cells: a critical signaling crossroad sustaining liver fibrosis. *Int J Mol Sci*. 2019;20(11):2700.
66. Kim J, Kim B, Kim SM, et al. Hypoxia-induced epithelial-to-mesenchymal transition mediates fibroblast abnormalities via ERK activation in cutaneous wound healing. *Int J Mol Sci*. 2019;20(10):2546.
67. Muchir A, Kim YJ, Reilly SA, Wu W, Choi JC, Worman HJ. Inhibition of extracellular signal-regulated kinase 1/2 signaling has beneficial effects on skeletal muscle in a mouse model of Emery-Dreifuss muscular dystrophy caused by lamin A/C gene mutation. *Skelet Muscle*. 2013;3(17):1-10.

68. Olson LE, Soriano P. Increased PDGFRalpha activation disrupts connective tissue development and drives systemic fibrosis. *Dev Cell*. 2009;16(2):303-313.
69. Wosczyna MN, Rando TA. A muscle stem cell support group: coordinated cellular responses in muscle regeneration. *Dev Cell*. 2018;46(2):135-143.
70. Feng J, Zhang Q, Mo W, et al. Salidroside pretreatment attenuates apoptosis and autophagy during hepatic ischemia-reperfusion injury by inhibiting the mitogen-activated protein kinase pathway in mice. *Drug Des Devel Ther*. 2017;11:1989-2006.
71. Thurairajah K, Briggs GD, Balogh ZJ. The source of cell-free mitochondrial DNA in trauma and potential therapeutic strategies. *Eur J Trauma Emerg Surg*. 2018;44(3):325-334.
72. Braian C, Hogea V, Stendahl O. Mycobacterium tuberculosis- induced neutrophil extracellular traps activate human macrophages. *J Innate Immun*. 2013;5(6):591-602.
73. Godsell J, Rudloff I, Kandane-Rathnayake R, et al. Clinical associations of IL-10 and IL-37 in systemic lupus erythematosus. *Sci Rep*. 2016;6:34604.
74. Manzenreiter R, Kienberger F, Marcos V, et al. Ultrastructural characterization of cystic fibrosis sputum using atomic force and scanning electron microscopy. *J Cyst Fibros*. 2012;11(2):84-92.
75. Cepika AM, Soldo Juresa D, Morovic Vergles J, et al. Decrease in circulating DNA, IL-10 and BAFF levels in newly-diagnosed SLE patients after corticosteroid and chloroquine treatment. *Cell Immunol*. 2012;276(1–2):196-203.
76. Jang CH, Choi JH, Byun MS, Jue DM. Chloroquine inhibits production of TNF-alpha, IL-1beta and IL-6 from lipopolysaccharide-stimulated human monocytes/macrophages by different modes. *Rheumatology (Oxford)*. 2006;45(6):703-710.
77. Cook KL, Warri A, Soto-Pantoja DR, et al. Hydroxychloroquine inhibits autophagy to potentiate antiestrogen responsiveness in ER+ breast cancer. *Clin Cancer Res*. 2014;20(12):3222-3232.
78. Ramser B, Kokot A, Metze D, Weiss N, Luger TA, Bohm M. Hydroxychloroquine modulates metabolic activity and proliferation and induces autophagic cell death of human dermal fibroblasts. *J Invest Dermatol*. 2009;129(10):2419-2426.
79. Avina-Zubieta JA, Johnson ES, Suarez-Almazor ME, Russell AS. Incidence of myopathy in patients treated with antimalarials. A report of three cases and a review of the literature. *Br J Rheumatol*. 1995;34:166-170.
80. Khosa S, Khanlou N, Khosa GS, Mishra SK. Hydroxychloroquine-induced autophagic vacuolar myopathy with mitochondrial abnormalities. *Neuropathology*. 2018;38(6):646-652.

SUPPORTING INFORMATION

Additional Supporting Information may be found online in the Supporting Information section.

How to cite this article: Edwards NJ, Hwang C, Marini S, et al. The role of neutrophil extracellular traps and TLR signaling in skeletal muscle ischemia reperfusion injury. *The FASEB Journal*. 2020;34:15753–15770. https://doi.org/10.1096/fj.202000994RR